# Multi-Agent Formation Tracking for Autonomous Surface Vehicles

Rasmus Ringbäck, Jieqiang Wei, Elias Strandell Erstorp, *Graduate Student Member, IEEE*, Jakob Kuttenkeuler, Tor Arne Johansen, *Senior Member, IEEE*, and Karl Henrik Johansson, *Fellow, IEEE*

***Abstract*— In this article, the problem of collaborative tracking of an underwater target using autonomous surface vehicles (ASVs) is studied. Distance-based formation control with a collision-avoidance potential function is employed as a solution. A formation control protocol is devised and applied to the formation tracking problem. With the protocol, the vehicles form a desired formation around a moving target in order to continuously estimate its position, while the centroid of the formation tracks the target. Almost global stability is proved for the case with three tracking agents. A fully operational platform with four ASVs was built to implement the derived algorithms. One of the vehicles was used to simulate a target and the rest to form a triangular formation around it. Power usage of a naval vessel is highly affected by water resistance forces which increases significantly with the velocity. This was accounted for by adding an additional term to the formation tracking protocol, thereby increasing the overall system endurance. Experimental results are presented.**

***Index Terms*— Autonomous surface vehicles (ASVs), formation control, multi-agent systems, tracking.**

## I. Introduction

### A. Background and Motivation

MONITORING of marine wildlife is important for both environmental and industrial concerns. Knowing movement patterns and discovering breeding grounds and spawns have great value for the research community. GPS tracking and other radio-based techniques have successfully been used to monitor the movement of larger sea creatures, such as whales and dolphins. However, these methods have the drawback of using both large transmitting devices and the inherent unreliability of communicating information under water. Usually, positioning of the animals can only be done at certain times when they surface. For aquatic animals that reside permanently underwater, such as fish or sharks, this is not a viable strategy.

Underwater surveillance and positioning is a challenging research area because of the high electromagnetic absorption of water, especially seawater with its high salinity. The solution has, for the most part, been to use acoustic measurement techniques, which can be either passive or active sonar. The drawback is the limited range, namely only the largest of animals, such as whales can be heard from more than a few miles away, and small acoustic tags generally have low power output. Hence, for accurate positioning, the use of closer range trilateration is necessary.

With the use of robotics, new possible ways to forward research in this area can be developed [1], [2]. There is a large potential use of *autonomous surface vehicles* (ASVs) and *autonomous underwater vehicles* to both observe and follow monitored animals in an autonomous manner. ASVs can estimate the location of an underwater target transmitting sound at regular intervals with the use of distance-of-arrival, directional finding, or triangulation techniques, for instance, studied in [3] and [4]. With a group of vehicles, as long as the target does not move much faster than the ASVs or dives too deep for the signal to reach the surface, the group would be able to continuously acquire new estimates by keeping themselves near the estimated locations. The challenge consists of providing a reliable control scheme for the vehicles, together with a robust communication network and a steady stream of localization estimates.

In this article, we will present a system of ASVs which can be used for monitoring of a target fitted with a small acoustic transmitter. One key aspect of ASVs is that the power usage is at least proportional to the square of the speed, which has to be taken into consideration to ensure the sustainability of the system.

### B. Related Literature

The design methodology in this article is closely related to multi-agent formation control which has been extensively studied in the last two decades [5], [6]. Smith *et al.* [7]

Manuscript received August 9, 2020; accepted October 8, 2020. Date of publication November 13, 2020; date of current version October 8, 2021. Manuscript received in final form October 30, 2020. This work was supported in part by the Knut and Alice Wallenberg Foundation, Swedish Research Council, in part by the Swedish Foundation for Strategic Research, in part by the Research Council of Norway [Norwegian University of Science and Technology (NTNU)-AMOS] under Grant 223254, in part by the Swedish Maritime Administration, and in part by the NTNU Centre for Autonomous Marine Operations and Systems. Recommended by Associate Editor A. Girard. *(Corresponding author: Jieqiang Wei.)*

Rasmus Ringbäck was with the School of Electrical Engineering and Computer Science, KTH Royal Institute of Technology, 100 44 Stockholm, Sweden. He is now with Saab AB, 175 41 Järfälla, Sweden (e-mail: ringback@kth.se).

Jieqiang Wei is with Ericsson AB, 115 41 Stockholm, Sweden (e-mail: jieqiang.wei@gmail.com).

Elias Strandell Erstorp and Jakob Kuttenkeuler are with the Centre of Naval Architecture, KTH Royal Institute of Technology, 100 44 Stockholm, Sweden (e-mail: eliasse@kth.se; jakob@kth.se).

Tor Arne Johansen is with the Center for Autonomous Marine Operations and Systems, Norwegian University of Science and Technology, 7491 Trondheim, Norway (e-mail: tor.arne.johansen@ntnu.no).

Karl Henrik Johansson is with the Division of Decision and Control Systems, School of Electrical Engineering and Computer Science, KTH Royal Institute of Technology, 100 44 Stockholm, Sweden (e-mail: kallej@kth.se).

Color versions of one or more of the figures in this article are available online at https://ieeexplore.ieee.org.

Digital Object Identifier 10.1109/TCST.2020.3035476

proposed a control strategy to make three agents converge to a designated triangular formation by using the distances between their neighbors and themselves. Convergence was shown to the desired distances except for initial conditions where all the agents are *collinear*. In [8], the same problem was addressed further, and Sun *et al.* [9] proved that under a gradient-decent-based control law, the system has a rank-preserving property. Rank-preserving means that when a formation has been initialized in a particular dimension, it cannot change to another dimension. For instance, a 2-D formation becoming 3-D or 1-D. We shall refer to this type of convergence as *almost global convergence*. Cao *et al.* [8] and Sun *et al.* [9] deal with formation control without collision avoidance. Convergence properties of distance-based formations, with collision avoidance, were studied in [10] and [11] without proof for the almost global convergence. Aforementioned works focus on holonomic agents. For formation control with nonholonomic agents, we refer to [12]–[15], and references within.

An application of multi-agent formation control is to estimate and track the position of an unknown target. When it comes to tracking and surveillance, having multiple vehicles taking measurements is beneficial. Accurate localization requires more than one measurement with sensors spread out to give as much coverage as possible, which reduces the sensitivity and increases the robustness of the system. With several agents, standard localization methods can be used, e.g., triangulation or trilateration. Using known information of a target, a target-capturing algorithm was proposed in [16] which guarantees that the centroid of the formation tracks the target and the agents circumnavigate around the target for all time. The idea of circumnavigation has been further used in additional articles for estimation of a target position. In [17], a method for localization was developed using the movement of the agent and continuous distance measurements of the target. A similar method was later developed in [18] and [19] for multi-agent systems. The essence of these methods is to guarantee a *persistent excitation* condition, crucial for adaptive identification schemes, by using circumnavigation of the agent around the estimated target. However, this is a drawback when considering surface vehicles since continuous circumnavigation comes with significant energy losses.

Practical implementations of multi-agent systems for localization and tracking have been published using various methods. For instance, Sharma *et al.* [20] used a scheme for distributed localization with bearing measurements using agents with wheel encoders and omnidirectional cameras. Mehrez *et al.* [21] developed a system using moving horizon estimation and nonlinear model predictive control for trajectory tracking and compared it with the more standard extended Kalman filter with promising results.

### C. Contribution

First, in this article, we present a reliable autonomous tracking system for underwater targets using ASVs with collision avoidance and the energy usage of the agents taken into consideration. The system and control protocol is implemented in a complete experimental system which shows the practical capability of the method.

Second, the convergence property of the proposed control protocol is proven analytically. If considering the case without the target in the formation, the proposed protocol is a distance-based formation control protocol using a collision-avoidance potential function [10], [11]. With three agents, the desired formation is achieved asymptotically for almost all initial conditions, i.e., *almost global stability*. Compared with [9] and [22], which depends on the analysis of the Hessian matrix of a potential function without collision avoidance, our method can be extended to arbitrary potential functions.

The stability of distance-based formation control protocols with more than three agents is still open [23]. However, we extend the three agent control protocol to the tracking problem and prove that the same stability properties hold.

### D. Organization

In Section II, some useful definitions are reviewed. The objective of this article is formulated in Section III. The formation tracking protocol is proposed and is proven to be almost globally stable in Section IV, using the proof of almost global stability of a distance-based formation control system with three agents presented in the Appendix. The experimental design for the system of ASVs and the results from experiments are presented in Sections V and VI, respectively. Then, this article is concluded in Section VII.

## II. Preliminaries

The notations used in this article are fairly standard. With $\mathbb{R}_-, \mathbb{R}_+, \mathbb{R}_{\geq 0}$ and $\mathbb{R}_{\leqslant 0}$, we denote the sets of negative, positive, nonnegative, and nonpositive real numbers, respectively. $\|\cdot\|$ denotes the $\ell_2$-norm. The operator col defines the stacked column vector. For a stacked vector $x = [x_1^\top, x_2^\top, \ldots, x_r^\top]^\top$ with $x_i^\top \in \mathbb{R}^l, i = 1, \ldots, r$, we define the block diagonal matrix $D(x) := \text{diag}\{x_i\}_{i=1,\ldots,r} \in \mathbb{R}^{rl \times r}$.

The notions about graph theory are consistent with [24]. An undirected *graph* $\mathcal{G} = (\mathcal{I}, \mathcal{E})$ consists of a finite set of nodes $\mathcal{I} = \{1, 2, \ldots, n\}$ and a set of edges $\mathcal{E} \in \mathcal{I} \times \mathcal{I}$ of unordered pairs of $\mathcal{I}$. To each edge $(i, j) \in \mathcal{E}$, we associate a weight $w_{i,j} > 0$. We denote the set of neighbors of node $i$ as $\mathcal{N}_i = \{j \in \mathcal{I} \mid w_{i,j} > 0\}$. If the edges are ordered pairs of $\mathcal{I}$, the graph $\mathcal{G}$ is called a *directed graph*, or *digraph* for short. An edge of a digraph $\mathcal{G}$ is denoted by $(i, j)$ (with $i \neq j$) representing the tail vertex $i$ and the head vertex $j$ of this edge. A digraph with unit weights is completely specified by its *incidence matrix* $B \in \mathbb{R}^{n \times m}$, where $|\mathcal{E}| = m$, with $B_{i,j}$ equal to $-1$ if the $j$th edge is toward vertex $i$, and equal to 1 if the $j$th edge is originating from vertex $i$, and 0 otherwise. The incidence matrix for undirected graphs is defined by adding arbitrary orientations to the edges of the graph.

*Definition 1 [25]:* We will say that the origin $x = 0$ is an *almost globally stable* fixed point for the system $\dot{x}(t) = f(x)$ if $f(0) = 0$ and almost all trajectories converge to it, i.e., if we note by $f^t(x_0)$ the trajectory at time $t$ that starts at $x_0$, then the set

$$\{x_0 \in \mathbb{R} \mid \lim_{x \to +\infty} f^t(x_0) \neq 0\}$$

has zero Lebesgue measure.

## III. Problem Formulation

In this article, we consider a problem of formation tracking applied to ASVs. A set of agents are designed to create a specified formation, while at the same time aiming to keep a moving target at the center of the formation. More precisely, we consider the system with $n$ agents with $x_i(t) \in \mathbb{R}^2, i \in \mathcal{I} := \{1, \ldots, n\}$ being the position of the agents, and $x_T(t)$ being the projected position of the underwater target on the surface. Any realizable formation is possible to use, but the final control aim is to let $x_i$ form a regular polygon with $x_T$ aligning with the centroid $x_c$ of this polygon. The reason for this aim is that with the target at the center of the polygon formation, we have better performance of source localization, i.e., the estimation of the target position [26]. Here, we assume that the position of the target is known to the agents, a premise based on the inclusion and accuracy of the localization algorithm.

The dynamics of the tracking agents are given as

$$\dot{x}_i = u_i, \quad i \in \mathcal{I} \tag{1}$$

where $u_i \in \mathbb{R}^2$ is the control input for the $i$th agent. Given an undirected graph $\mathcal{G} := \{\mathcal{I}, \mathcal{E}\}$, the desired formation of the agents can be defined accordingly as

$$\Phi \triangleq \{x \in \mathbb{R}^{2\cdot n} \mid \|x_i - x_j\| = d_{i,j} \quad \forall (i, j) \in \mathcal{E}\}, \tag{2}$$

where $d_{i,j}$s are the desired realizable distances between the agents. We furthermore assume that the formation $\Phi$ is rigid. An illustration of the formation tracking problem can be seen in Fig. 1. When the target is absent, the formation tracking problem degenerate to ordinary formation control, i.e., design the input $u_i$ such that the positions of the agents achieve the desired formation $\Phi$.

The control objective is the design and implementation of a distance-based formation tracking protocol, using collision-avoidance potential functions. The objective is further expanded more explicitly to ASVs, incorporating the above-mentioned tracking protocol with the additional aim of increasing system endurance. The power to speed ratio on the water is at least quadratic; therefore, for ASV agents with low energy storage, lower speeds are highly desirable. Operational loss of one or more agents would cause poor accuracy for further localization of the target, making energy management an important consideration.

## IV. Formation Tracking With Trilateration

In this section, we consider the formation tracking problem and propose our control protocol and the adaption to the experimental system.

First, we review an existing formation control algorithm commonly used in the literature, for example, in [8] and [9]

$$\dot{x}_i = -\sum_{j \in \mathcal{N}_i} \left(\|x_i - x_j\|^2 - d_{i,j}^2\right)(x_i - x_j), \quad i \in \mathcal{I} \tag{3}$$

with $x_i \in \mathbb{R}^2$ is the steepest descent gradient flow of the potential function

$$V_{col}(x) = \frac{1}{4} \sum_{(i,j)\in\mathcal{E}} \left(\|x_i - x_j\|^2 - d_{i,j}^2\right)^2. \tag{4}$$

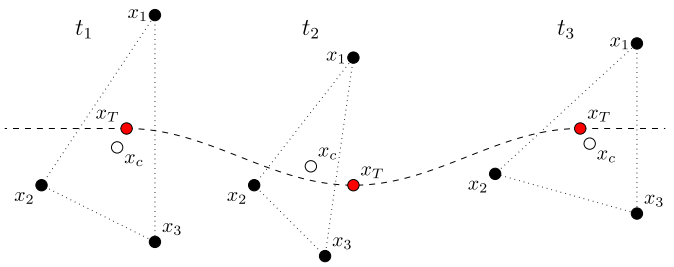


Fig. 1. Illustration of how the three agent formation tracks the target moving along a trajectory. The agents $x_i$, $i = 1, 2, 3$, with the centroid $x_c$, are given over three-time steps together with the target estimations $x_T$ in red. By the agents forming the desired formation $\Phi$, and where the centroid attempts to align with the target estimation, the system is able to acquire sufficient localization ability to keep tracking the target.

However, this protocol cannot guarantee collision avoidance.

In this article, we focus on the following collision-avoiding potential function [10]

$$V(\mathbf{x}) = \sum_{(i,j)\in\mathcal{E}} \gamma\left(\beta_{i,j}(\mathbf{x})\right) \tag{5}$$

where $\gamma(\beta_{i,j}) = (((\beta_{i,j} - d_{i,j}^2)^2)/\beta_{i,j})$ and $\beta_{i,j} = \|x_i - x_j\|^2$.

We define $z = (B^\top \otimes I_2)x$, $D(z) = \text{diag}(z_1, z_2, \ldots, z_m)$ and $\mathcal{D}(x) = \text{col}(\|x_i - x_j\|^2, (i, j) \in \mathcal{E})$, where $B$ is the incidence matrix of the graph representing the rigid formation. Denote the rigidity matrix as

$$R(z) = \frac{1}{2}\frac{\partial \mathcal{D}}{\partial x} \tag{6}$$

$$= D(z)^\top (B^\top \otimes I_2). \tag{7}$$

We further define $e = [\rho_1, \ldots, \rho_m]^\top$, where $\rho_k = (\partial\gamma/\partial\beta_{i,j}) = ((\beta_{i,j}^2 - d_{i,j}^4)/\beta_{i,j}^2)$, for $k = (i, j)$. Then, the dynamic of the agents, which is the steepest descent gradient flow of the potential function (5), can be written in a compact form as follows [9]:

$$\dot{x} = -R^\top(z)e \tag{8}$$

$$= -(B \otimes I_2)D(z)e. \tag{9}$$

Furthermore,

$$\dot{z} = (B^\top \otimes I_2)\dot{x} \tag{10}$$

$$= -((B^\top B) \otimes I_2)D(z)e. \tag{11}$$

It can be readily checked that the centroid of the agents is invariant.

*Remark 2:* Notice that if the relative distance $\beta_{i,j}$ becomes zero, then $V(\mathbf{x})$ is equal to infinity. Furthermore, for the system controlled by (8), we have $\dot{V}(\mathbf{x}) \leq 0$. Hence, collision is avoided for all times.

The local stability of (8) was proved in [10]. However, *almost global stability*, even for three agents, cannot be found in the literature. In this article, we present a proof for the case of three agents, which can be found in the Appendix.

Next, we propose a protocol based on the collision-avoiding potential function (5) and the dynamic (8) for the formation tracking problem, i.e., surrounding the target.

Consider the dynamics of the agents as given by

$$\dot{x}_i = v_T - (x_c - x_T) - \sum_{j\in\mathcal{N}_i} \rho_k(x_i - x_j), \quad i \in \mathcal{I} \tag{12}$$

where $x_c = (1/n)\sum_{i\in\mathcal{I}} x_i$ is the centroid of the agents, and $x_T \in \mathbb{R}^2$ and $v_T \in \mathbb{R}^2$ are the position and velocity of the target, respectively, which are assumed to be known. The stacked version of the system is written as

$$\dot{x} = \mathbb{1} \otimes (v_T - (x_c - x_T)) - \nabla V(x). \tag{13}$$

Determining the number of incorrect formations[1] for multi-agent systems with more than three agents is still an open problem in the literature [23]. The system (12) can be seen as an extension of the three agent problem with tracking terms. Based on the proof in the Appendix, we shall prove the almost global convergence of this system with a triangular formation.

*Theorem 3:* Consider the system (12) with three agents and assume that the desired triangle formation is realizable. If one of the following holds:

1) the initialization of the agents is generic;
2) the initialization of the agents is collinear, i.e., there exists a line $\eta$ such that $x_i(0) \in \eta \subset \mathbb{R}^2, i = 1, 2, 3$, and there exists a $t \geq 0$ such that $x_T(t) \notin \eta$.

Then, the desired formation is achieved with the centroid tracking the target asymptotically.

*Proof:* The proof can be divided into two steps.

In the first step, we prove that the centroid is converging to the target asymptotically. In fact, the dynamic of the centroid is given as

$$\dot{x}_c = v_T - (x_c - x_T). \tag{14}$$

Then, the convergence is clear by considering the Lyapunov function $V(x_c) = (1/2)\|x_c - x_T\|^2$, where the time derivative satisfies that $\dot{V} = -2V$.

In the second step, consider the coordination error denoted as $\tilde{x}_i = x_i - x_T$ whose dynamic is given as

$$\dot{\tilde{x}}_i = -(\tilde{x}_c) - \sum_{j\in\mathcal{N}_i} \rho_k(\tilde{x}_i - \tilde{x}_j), \quad i \in \mathcal{I} \tag{15}$$

where $\tilde{x}_c = x_c - x_T$. Notice that if there exists a line $\eta$ such that $x_i(0) \in \eta \subset \mathbb{R}^2, i = 1, 2, 3$ and $x_T(t) \in \eta, \forall t \geq 0$, then this line $\eta$ is invariant for the system (12). Then, the conditions 1) and 2) guarantee that there exists a $t \geq 0$ such that the vectors $\tilde{x}_i, i = 1, 2, 3$ are not collinear. In this case, we prove that $\tilde{x}_i, i = 1, 2, 3$ cannot converge to a line.

By the convergence of $x_c - x_T$, we have $\tilde{x}_c(t) \to 0$ as $t \to \infty$. Then the equilibrium set of the error dynamic is given as

$$\tilde{\mathcal{H}} = \{\tilde{x} \in \mathbb{R}^6 \mid R^\top(\tilde{z})e = 0\} \tag{16}$$

where $\tilde{z} = (B^\top \otimes I_2)\tilde{x}$, and the sets of correct and incorrect equilibria are, respectively, denoted as

$$\tilde{\mathcal{H}}_c = \{\tilde{x} \in \mathbb{R}^6 \mid R^\top(\tilde{z})e = 0, e = 0\} \tag{17}$$

$$\tilde{\mathcal{H}}_i = \{\tilde{x} \in \mathbb{R}^6 \mid R^\top(\tilde{z})e = 0, e \neq 0\}. \tag{18}$$

[1]For the definition of incorrect formations, refer to [23].

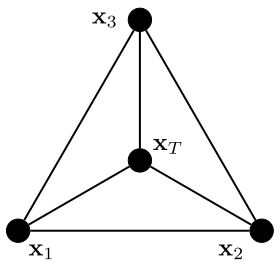


Fig. 2. Graph structure used for three agents with target.

Furthermore, by the same argument as in the proof of Theorem 8 from the Appendix, i.e., using $\tilde{W} = \|\tilde{x}_1 - \tilde{x}_2\| + \|\tilde{x}_2 - \tilde{x}_3\| - \|\tilde{x}_3 - \tilde{x}_1\|$, the convergence to $\tilde{\mathcal{H}}_c$ can be proved if there exists a $t \geq 0$ such that the vectors $\tilde{x}_i, i = 1, 2, 3$ are not collinear. □

*Remark 4:* From the proof Theorem 3, we note that the dynamic of the error (15) is gradient decent of the following potential function:

$$V_t := V_1 + V \tag{19}$$

where $V_1 = (1/2n)\|\sum_{i\in\mathcal{I}} \tilde{x}_i\|_2^2$. More specifically, in this section, we set $n = 3$. The graph structure can be seen in Fig. 2.

### A. Adaptation to the Experimental System

In principle, the control protocol (12) can be applied to the ASVs directly. However, the power usage for an ASV is proportional to the resistance force acting on the vessel. The simplest derivation of the resistance from Bernoulli's principle [27] gives that the resistance can be described by $R = (1/2)\rho C A v^2$, where $\rho$, in this case, denotes fluid density, $C$ is the coefficient of drag, $A$ is the surface area, and $v$ is the velocity. The energy consumption then increases with the square of the velocity, which, thus, is critical to decreasing. In order to prolong the potential operational time, we shall present an adaptation of the above-mentioned control protocol (12), which will be used by the ASVs in the experiment.

In the experiment, the velocity of the target is not available directly, instead the position of the target is measured, using trilateration, every $\tau$ time steps. In other words, for any $t \geq t_0$, $[x_T(t_0), x_T(t_0 + \tau), \ldots, x_T(t_0 + N\tau)]$ is available, where $N = \lfloor((t - t_0)/\tau)\rfloor$. To abbreviate notations, we denote the target $x_{T,N} := x_T(t_0 + N\tau)$ and the position of the agents as $x_{i,N} := x_i(t_0 + N\tau)$. From the time $t_0 + N\tau$ to $t_0 + (N + 1)\tau$, the agents are designed to achieve the desired formation. More precisely, the dynamic of each agent is given as

$$\begin{aligned}\dot{x}_i(t) = &-(x_c(t) - x_{T,N}) - \sum_{j\in\mathcal{N}_i} \rho_k(x_i(t) - x_j(t)) \\ &- \alpha_i(x_i(t) - x_{i,N}), \quad i \in \mathcal{I} \\ &t \in [t_0 + N\tau, t_0 + (N + 1)\tau]\end{aligned} \tag{20}$$

where $\alpha_i$ is a positive parameter.

*Remark 5:* By denoting the state error $\tilde{x}_i = x_i - x_{T,N}$ and $\tilde{x}_{i,N} = x_{i,N} - x_{T,N}$, the error dynamic is given as

$$\dot{\tilde{x}}_i = -\tilde{x}_c - \sum_{j \in \mathcal{N}_i} \rho_k(\tilde{x}_i(t) - \tilde{x}_j(t)) - \alpha_i(\tilde{x}_i - \tilde{x}_{i,N})$$

where $\tilde{x}_c = (1/n)\sum_{i\in\mathcal{I}} \tilde{x}_i$. The above-mentioned dynamic (20) is the gradient decent algorithm of the following potential function:

$$V_{\text{tot}} := \frac{1}{2n}\sum_{i\in\mathcal{I}} \|\tilde{x}_i\|_2^2 + V(\tilde{x}) + \sum_{i\in\mathcal{I}} \frac{\alpha_i}{2}\|\tilde{x}_i - \tilde{x}_{i,N}\|_2^2$$

where $V$ is given as in (5). It can be seen that this potential function $V_{\text{tot}}$ takes the distance between the centroid of the formation and $x_{T,N}$, collision avoidance, and the distance between $x_i$ and $x_{i,N}$ into consideration.

The last term of the potential function $V_{\text{tot}}$ punishes the distance between the current agent position $x_i$ and the position of the agent at the next sampling time $x_{i,N}$. By introducing this term, the cost of movement for individual agents can be managed. Increasing $\alpha_i$ makes the agent stay closer to its current position, and thus, lower speeds and less energy will be used. With the same value of $\alpha_i$ for all agents, the system would be affected uniformly. But with individually different values, certain agents would move slower than others. However, any increase of $\alpha_i$ will potentially cause worse tracking ability of the whole system. In the current system, the values of $\alpha_i, i = 1, 2, 3$ is set by the operator and not dependent on any other system variable.

The separation of the desired agent states and current positions, through which we can include the term $\alpha_i(\tilde{x}_i - \tilde{x}_{i,N})$ in (20), was inspired by [13]. For the system (20), a potential proof of the almost global stability would be significantly more difficult than the case of (12). In the following subsections, we shall present a physical system using ASVs, where the trajectory generated by (20) will be used as a control reference. The used formation was in this case an equilateral triangle, i.e., $d_{i,j} = d, \forall i, j$.

## V. ASV Platform Setup

Based on the devised control law, an algorithm was implemented in a system of small ASVs. Four vehicles were employed for a series of experiments. Three of these vehicles took the role of the controllable agents $x_i, i = 1, 2, 3$, aiming to create the triangular formation around the target. The fourth agent was manually controlled and carried an acoustic transmitter attached to a rigid pole below the water surface, thus emulating the behavior of a fish and acting as the target $x_T$. The task of the system was to continuously track the target using receivers on the other vehicles. The position of the target was estimated using trilateration every 8 s, i.e., we set $\tau = 8$.

### A. Ducklings

At Maritime Robotics Laboratory, KTH Royal Institute of Technology, Stockholm, Sweden, four ASVs were constructed. They are small catamarans driven by two external thrusters at the back of the vehicles. Due to their small size, they are capable of agile steering and high initial acceleration. In Fig. 3, an image of the "ducklings," a name which will be used when referring to the ASVs, can be seen. In Table I, specifications have been listed.

Fig. 3. ASVs used in the experiments. The left and right pictures show the front and back of the "ducklings," where the acoustic receivers and thrusters, RFD868 and Wifi antennas can be seen, respectively.

TABLE I
TECHNICAL SPECIFICATIONS OF THE DUCKLINGS

| Parameter | Value |
|---|---|
| Length | 1120 [mm] |
| Breadth | 720 [mm] |
| Height | 240 [mm] |
| Weight | 15 [kg] |
| Material | Polystyrol |
| Thrusters | BLUE ROBOTICS, T200 |
| Operational speed | 1 [m/s] |
| Maximum speed | 1.5 [m/s] |
| Battery type | 6S LiPo |
| Battery capacity | 16 or 32 [Ah] |
| On-board PC | Raspberry Pi 3 Model B (Raspbian OS) |
| Microcontroller | Custom Arduino Due (ARM Coretex M3) |
| GPS antenna | Dielectric GPS/GLONASS |
| Radio | Ubiquiti Bullet M5Ti |
| Radio antenna | 5 GHz, 8 dBi |
| Wireless protocol | AirMax |

On land two PC's were used, one for running the formation controller and one for controlling the target ASV. The PC's were connected to the network of vehicles through a base station via a switch. Low-level control of a vehicle was handled by a microcontroller unit (MCU). The MCU handles navigation and path-following through GPS and an inertial measurement unit (IMU) and reacts to a limited set of commands. To establish a network of vehicles, they were each equipped with an embedded Linux computer and wireless modems. This setup is required to make use of the LSTS Toolchain. A schematic of the system can be seen in Fig. 4.

*1) LSTS Toolchain:* The open-source LSTS Toolchain [28] for control of systems of autonomous vehicles were used as the software platform for the experiments. The toolchain provides three main components: *Neptus*, a user interface for situation awareness, mission control and logging. *DUNE* is an on-board software running mission-execution, systems monitoring, sensor data collection, and logging in parallel processing threads called tasks. And the *intermodule communication protocol* (IMC) is a message-based protocol for sharing information between processes and systems in a publish-subscribe pattern.

The toolchain provided a well-defined framework for communication and execution between different modules. Different parts of the software could be developed in parallel without the need for extensive collaboration between the different geographically spread out participants in the project.

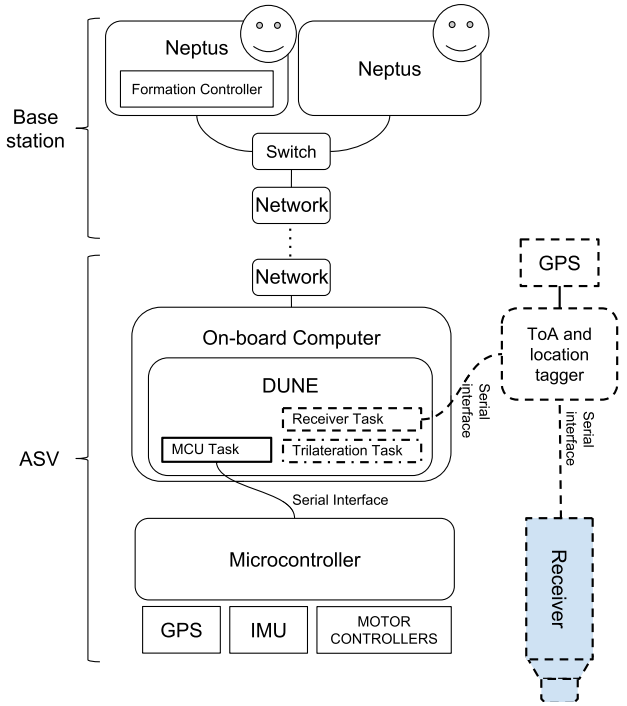


Fig. 4. Overview of the system during operation. Dashed lines denote subsystems and processes used only in agents. The dot-dashed line denotes the trilateration process running in the target.

The integration process, thus, became simple when the different modules were to be combined for the full experiment.

*2) DUNE:* The ducklings have integrated with the LSTS Toolchain by constructing a task in DUNE for interfacing with the on-board microcontroller. DUNE and the microcontroller were communicating through the MAVlink protocol [29] over a serial interface. MAVlink has a small overhead, suitable for low-bandwidth communication channels. The module keeps track of the vehicles current state and passes data by broadcasting IMC messages on the network. It also forwards commands, such as waypoints, to the MCU.

One DUNE task was responsible for interfacing data from the time of arrival (ToA) and location tagger. This task was only active in the three tracking vehicles that were equipped with acoustic receivers. It utilized GPS for reference and had an accuracy of $\sim$1 ms and $\pm$2 meters. The task was developed at the Norwegian University of Science and Technology (NTNU), Trondheim, Norway, which also owns and manages the acoustic equipment. A custom text-based protocol was used over this serial interface.

*3) Communication:* A network was established using five Ubiquiti Bullet M5Ti radios, each with a pair of 8-dBi antennas attached. All ducklings were equipped with a radio, and another one was used as a base station on land. The range of the network was limited mainly by environmental factors and antenna placement. The allowable ranges for the network to stay robust were determined by trial and error to be up to 500–600 m and were a limiting factor in the experimentation.

*4) Acoustic Transmitter:* The transmitter was a small acoustic fish-tag designed by Thelma Biotel. There are various types of transmitters available, but the model used in these

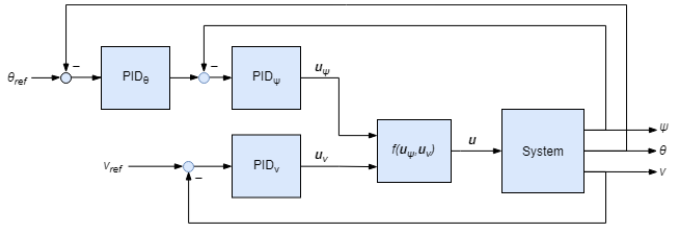


Fig. 5. Block diagram of the low-level control used by the ducklings. $\theta_{\text{ref}}$ is the absolute bearing toward the coordinate $\mathbf{x}$, $\theta$ the current bearing and $\psi$ the yaw rate. $\mathbf{u}$ is the combined inputs to the thrusters used both for yaw and forward propulsion $v$.

experiments was an ADT-16 which periodically sends its ID and depth. The transmitters are 70 mm in length and 16 mm in diameter. The tag is operating at a narrowband frequency centered around 67 kHz. The period between transmissions was set to 8 s. Range depends on several environmental factors but in good conditions 500–1000 m is expected.

*5) Acoustic Receiver:* The Thelma Biotel TBR 700 RT was used as a compatible receiver, where RT is short for real-time. The real-time feature of these receivers was necessary for the experiments as it made it possible to make accurate time stamps of the received signal. Accurately determining the ToA of the signal is a requirement for the localization to work. The measurements of the receivers are 230-mm length, 75-mm diameter, and 1140 grams.

*6) Low-Level Control and Path Following:* Through the MCU, the ducklings could control their navigation autonomously and employ basic path following, either on predefined trajectories or toward specific waypoints. From, for instance, $x_{i,N}$ and $x_i$ in the formation control algorithm, $\theta_{i,\text{ref}}$ was calculated as the reference bearing angle between the two coordinates. Using two cascaded PID-loops, input to the two thrusters at the back of the vehicle were given to control the yaw $\psi$ and direct the vehicle toward $x_i$.

The forward propulsion was set as $v_{i,\text{ref}}$ and was held by the use of a third PID-loop. Since the two thrusters have limited power output, a weighting had to be applied for high yaw rates. In that case, the yaw got priority over the forward propulsion until the desired heading was reached. An explaining figure of the control chain for one duckling can be seen in Fig. 5.

To limit unnecessary power usage, the positional control is not activated if the duckling is close enough to its goal. In this case, inside is a 5-m radius. Control of the ducklings could also be performed manually via radio transmitters. This was very useful for the times when network communication was lost and the ducklings needed to be driven closer or retrieved.

### *B. Implementation of the Control Algorithm*

Every time $t_0 + N\tau$, the measured states $x_{i,N}$, $i = 1, 2, 3$ and $x_{T,N}$ were made available in the network through DUNE. The next iterations $x_i$ of (20) were calculated by optimizing over the potential function $V_{\text{tot}}$ on a separate computer running the interface program Neptus. The result served as command instructions for the ducklings over the remainder of $t_0 + N\tau$ until $t_0 + (N+1)\tau$. The optimization algorithm was written in Java and used the nonlinear least square Levenberg–Marquardt

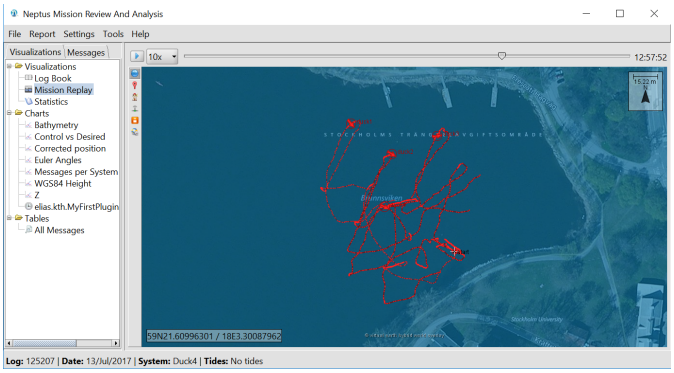


Fig. 6. Example of how the reviewing interface looks in the software Neptus, taken from one result of a preliminary test close to KTH Royal Institute of Technology, Stockholm, Sweden.

Fig. 7. Three of the "ducklings" out on the water.

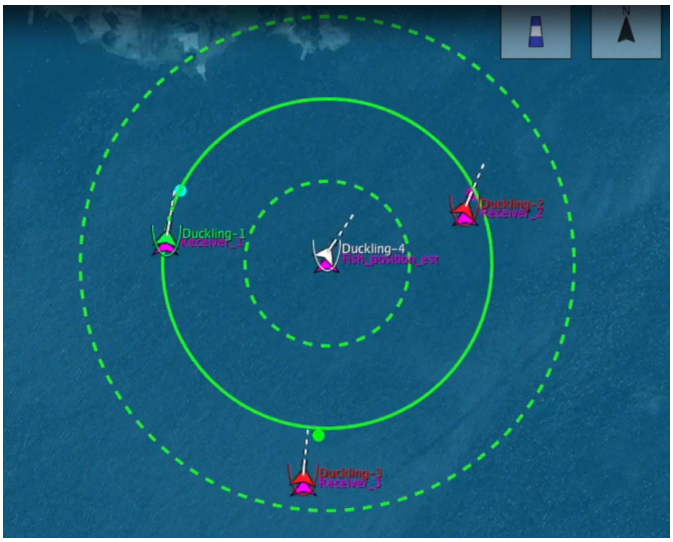


Fig. 8. Partial screen capture of the interface in Neptus during the execution of the experiment. The colored dots are current values of $x_i$, while the arrows are actual positions $x_{i,N}$ of the ASVs with attached receivers. The full green circle is the current radii of $\Phi$, i.e., the desired distance from agent to target.

solver included in the open-source apache commons math package.

*1) Target Localization:* In addition, at each time $t_0 + N\tau$, the state of the target $x_{T,N}$ was trilaterated using the time-stamped data from the other instances of DUNE in the network, implemented as its own task. Using three agents, time-difference-of-arrival could be utilized for the localization. The used algorithm employs a three-stage Kalman filter cascade [30]. The method relates to extended Kalman filtering and has the advantage that convergence can be guaranteed under mild assumptions.

*2) Neptus:* High-level control and monitoring of the ducklings were achieved through the command and control program Neptus, part of the LTST Toolchain. The formation control algorithm was designed as a module that can be turned ON and OFF inside the program, and where parameters, such as $\alpha_i$ and formation distances, can be changed.

Neptus gathers all data from nodes in the network, and any computer with Neptus can send control instructions to any vehicle with DUNE. The data are recorded and can be reviewed and analyzed, for instance, y replaying the whole experiment. Being able to have multiple simultaneous instances of Neptus was reassuring since there was less risk of potentially losing important data. In Fig. 6, an image can be seen of the reviewing interface.

## VI. Experiment

A series of tests were performed at Lännerstasundet, Stockholm. Four ASVs were employed, and the manually controlled ASV acted as the target by carrying the acoustic transmitter. Target estimations were performed and recorded every 8th s, and the positions of the ASV agents recorded every 2nd seconds. Several different sizes of the equilateral triangle formation were used. An image from the tests can be seen in Fig. 7.

The objective of the test was to evaluate the full-scale system with the two main components, i.e., the formation control algorithm and the location estimation algorithm. The formation control algorithm had ahead of time been applied to the ASVs and tested on its own, which was very useful for properly adapting the system before the full-scale integration. The accuracy of the tracking was evaluated by the fact that the absolute position of the ASV carrying the transmitter was known. An image of the interface in Neptus can be seen in Fig. 8 to better visualize how the system operated.

The navigational performance of the ASVs became degraded somewhat after several hours in the water, causing a slight difference in handling between them. In addition, the internal compass often did not provide an accurate heading, making the ASVs behave erratically before gaining enough speed to use the GPS trajectory. But overall, the ducklings were a useful test platform because of their agility and appropriate size. Larger vehicles would be harder to handle and transport, and smaller vehicles affected more by the sea state. The future addition of differential GPS with compass heading and improvement of the integrity of the hull would improve the robustness of the platforms.

### A. Results

The system was running successfully for several hours on the last day of experimentation. Three types of collected results will here be presented.

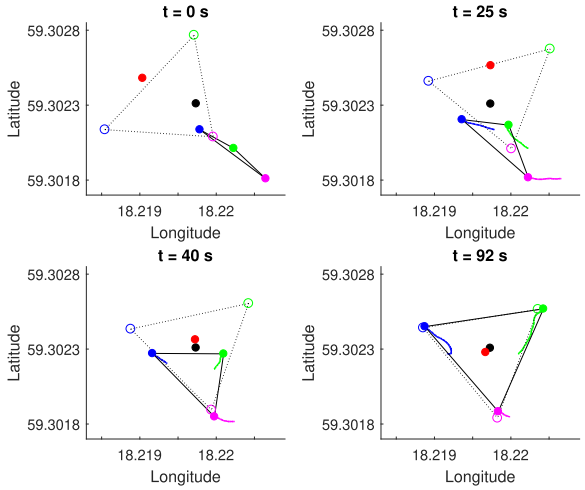


Fig. 9. Experimental result showing how the agent formation converges to the desired distances, while the estimated target position goes toward the actual. The ducklings (blue, green, and magenta dots) start in almost collinear positions with the target (black), which gives a bad estimated target position (red). The desired agent positions (circles) are calculated from the current positions. As time increases, the actual agents converge to a better formation and the estimation error decreases. Four steps of the process are shown.

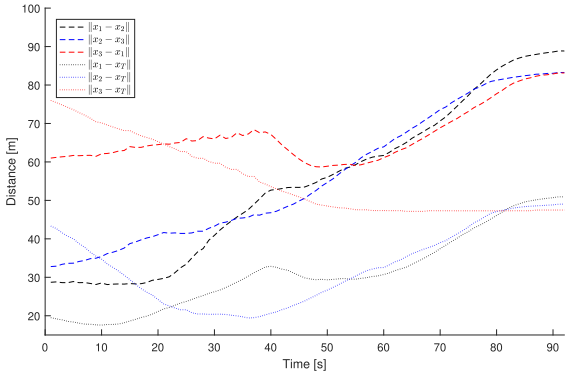


Fig. 10. Plot of the errors of the formation when converging to surround the target. The distance between the ASVs and the actual position of the target goes to toward the set distance of $r = 50$ meters, while the distances between each ASV goes toward $d_{i,j} = d = \sqrt{3}r$.

At time $t = 0$ in Fig. 9, we can see how the agents start in suboptimal initial positions where they are almost collinear. The estimation $x_{T,N}$ of the target is initially inaccurate, but the estimation error decreases as the agents move closer to the desired formation. Fig. 10 shows the formation convergence by which the result from Section IV is demonstrated. It was shown that a system of agents under the given control law (12) would converge to the formation $\Phi$ (2) for any noncollinear initial state. In fact, a collinear initial state would be impossible to achieve in a setting affected by any type of disturbances. The experiment also shows that the error between the estimated state of the target $x_{T,N}$ and the formation centroid $x_c$ decreases and eventually aligns when the formation converges.

Fig. 11 shows an experiment for a longer continuous time. The addition of the term $\alpha_i, i = 1, 2, 3$, added to the agent dynamics (20), was here evaluated as a proof-of-concept by manually increasing the value for the blue agent until sufficient effect was observed. The resulting trajectory became shorter,

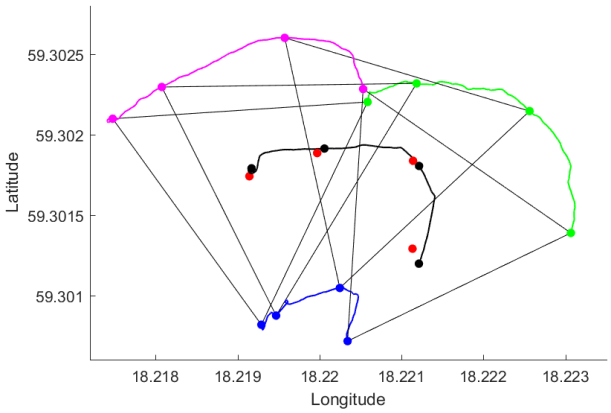


Fig. 11. Tracking of the moving target during several minutes, from the leftmost position to the lower right at four time steps. Actual position in black and estimated in red. The agents are able to follow the target and adapt their movement based on the weights $\alpha_i$.

and as can be seen, the whole formation rotated clockwise. The purpose of having control over this variable was to potentially decrease the energy usage in the affected agent. Losing one agent because of lack of energy would mean that the tracking system would be unable to continue operating. Adaptively changing the value of a time-variant $\alpha_i(t)$ for each agent would be a way to improve the system performance, for instance, by connecting it to measured fuel levels.

In Fig. 12, a plot of the error between the estimated target position and the measured value of the carrying agents position can be seen with the formation radius set to $r = 50$ m. The value of $r$ was set by changing the definition of $\Phi$, which for this formation had $d_{i,j} = d = \sqrt{3}r$. Since the recording frequency of the target estimation was lower than for the carrying agent position, the plot gets a saw-tooth shape. The path of the target can be seen in the lower figure. The plot shows that the estimation error never went above the in-radius 25 m, meaning that the target estimation did not risk leaving the interior of the formation. Two distinct regions can be seen. One with the higher error where the target traveled along a continuous trajectory and one with slightly lower errors where it only made small movements, distinguished by the short and jagged appearance. The first case was the most important since this was when the target could potentially escape if the error kept growing.

The tracking worked successfully for both smaller and larger formations. In Fig. 13, the estimation error can be seen for two additional test runs, now with radius 25 and 100 m. Both tests began from positions where the target was relatively stationary, which can be seen in the low error for the first 300 s in the 100-m test. Apart from the slightly larger error at the beginning of the 25-m test, the values of the errors are comparable between all three shown tests. However, the smaller the formation, the easier it would be for the target to leave the inside of the formation, creating a perhaps irreversible feedback loop of increasingly worse estimations. Larger formations would decrease this possibility but with instead the problem of more attenuated signals, where radii up to 150 m were tried successfully in these tests. The upper limit was in our case not determined by the range of the acoustic

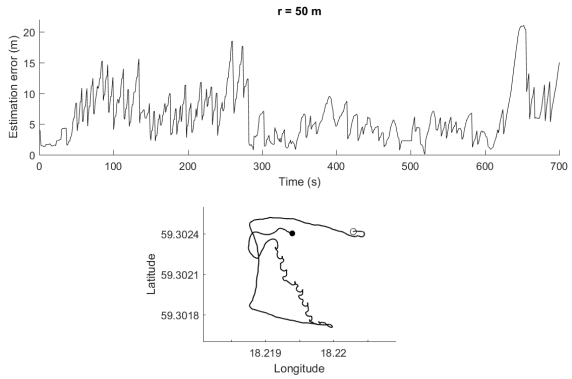


Fig. 12. Plot of the error between the actual and estimated target position over 700 s with the desired formation with a 50-m radius. The path of the target in the lower figure. Initial and final positions as circle and dot, respectively.

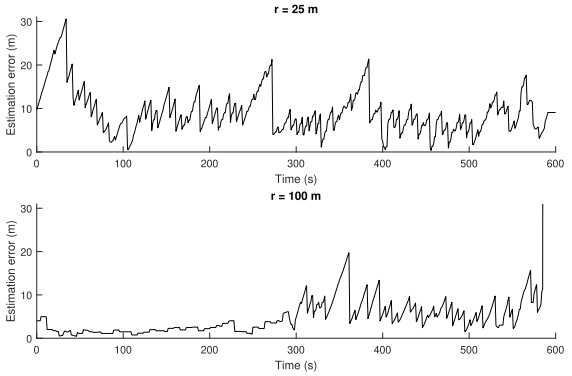


Fig. 13. Plot of the error of the estimated target position for two additional test runs, with the radius of the desired formation at 25 and 100 m, respectively.

transmitter but by the failure of the communication network over too large distances. This can, for instance, be seen at the end of the 100-m test. Communication was lost to one agent, and by the result, the estimation error kept growing to unrecoverable levels.

Although the achieved distances between agents were very promising, for future studies, the network stability and range should be improved. How the system would be able to handle the loss of the acoustic transmitter signal by one or more agents would be an interesting factor to investigate. A related factor would also be different repetition frequencies of the transmitter, where long periods of silence would set an upper limit on system performance. Moreover, how the system could incorporate time-varying formations would be studied in the future as well.

## VII. Conclusion

This article has investigated a novel approach to tracking of underwater targets with the use of ASVs. By creating a formation around the target with the vehicles, we were able to provide a setting from which a trilateration algorithm could be used to localize the target. Doing this continuously, the formation of agents was able to adapt so that the target was not lost.

The main focus has been on the control algorithm of the agents and their applications. It was proven that a system consisting of three agents forming a triangle formation had the property of almost global stability under the stated control law, a result not found in the previous literature for potential functions with collision avoidance. Through an extension of the control law, where the formation centroid was made to track the target, it was possible to apply the result to the tracking problem. Application to a system of real ASVs was then realized, providing a way to verify the performance and show the potential of the method.

Experiments performed showed that the method was viable and continuous tracking was possible without losing the target for extended periods of time. The constructed vehicles were also shown to be reliable in the performance of the task. Used as a target was, in this case, a small acoustic receiver fastened below a fourth vehicle. This simulated the behavior of a fish. For future development of the method, plans are to use real fish as the target. This would show the performance when faced with highly erratic behavior, now also with changes in depth, in a realistic scenario. If successful, larger scale utilization can be considered.

## Appendix
## Stability of the Formation Without the Target

In this appendix, we shall prove that for a three agent (realizable) triangle formation using control protocol (8), the desired formation is *almost globally stable*. Note that the system (8) is autonomous. Since a full stability analysis of the formation control problem with an arbitrary number of agents is still an open problem, we only consider the case with three agents, i.e., $n = 3$.

Using the potential function (4), the almost global convergence to the desired formation with three and four agents have been developed in [9] and [22]. Moreover, the analysis there was based on the Hessian matrix of the potential function; hence, it cannot be extended easily to the control law based on the potential function (5).

In this analysis, we re-index the edges as $1 = (1, 2), 2 = (2, 3), 3 = (3, 1)$. By using the same reasoning as in [9], the rank preserving is guaranteed. Indeed, denote $X = [x_1, x_2, x_3]$ and $Z = [z_1, z_2, z_3]$, where both belong to $\mathbb{R}^{2\times 3}$, the system (8) can be rewritten as

$$\dot{X} = -XE^{\top} \tag{21}$$

where $E = B\bar{E}B^{\top}$ and $\bar{E} = \text{diag}(e) = \text{diag}(\rho_1, \rho_2, \rho_3)$. The dynamic of $Z$ follows $\dot{Z} = -Z\bar{E}B^{\top}B$. Hence, by [31, Ch. 5, Lemma 1.22], we have that for any realizable formation and finite-time interval $I$, $\text{rank}(Z(t)) = \text{rank}(Z(0))$ for $t \in I$. However, as pointed out in [9], $\text{rank}(Z(t))$ can be degenerated as $t \to \infty$, especially if the formation is not realizable. See the following example.

*Example 6:* In this example, we present two simulations of the system (21). In Fig. 14, we implement the protocol to achieve an unrealizable formation with lengths of the edges equal to 1, 1, and 5. The empty circles and solid circles are the initial and final positions of the agents, respectively. The dashed arc is a line segment between the final positions of the agent 1 and 3.

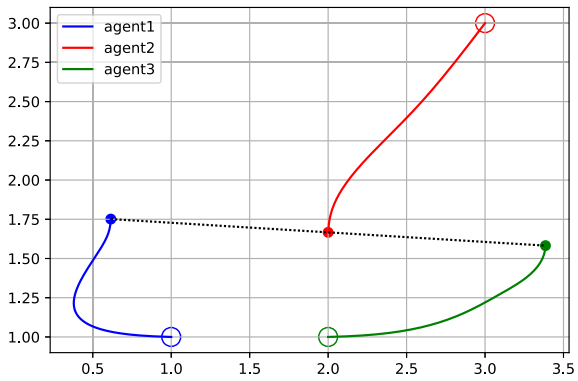


Fig. 14. Simulation of the protocol (21) with unrealizable formation.

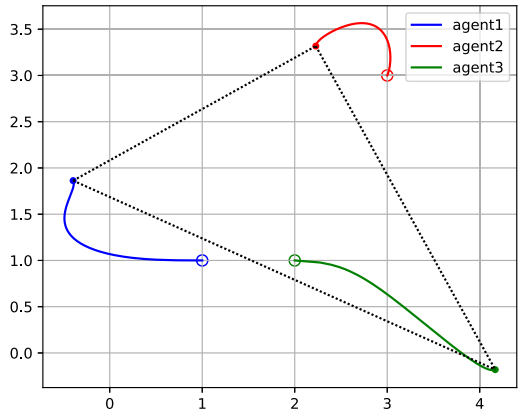


Fig. 15. Simulation of the protocol (21) with realizable triangular formation.

In Fig. 15, the same protocol is implemented to achieve a realizable triangular formation, with lengths of the edges equal to 3, 4, and 5, which is plotted as the dashed line segments.

To begin the proof, we first recall the following result from [10], which is not limited to the case with three agents.

*Lemma 7:* Consider the system (8) and assume the formation graph is connected, then $u_i \to 0$ as $t \to \infty$ for all agents.

The set of the equilibrium of (8) is denoted as

$$\mathcal{H} = \{x \in \mathbb{R}^6 \mid R^\top(z)e = 0\} \tag{22}$$

where $R(z)$ is defined as in (6), and the sets of correct and incorrect equilibria are denoted as

$$\mathcal{H}_c = \{x \in \mathbb{R}^6 \mid R^\top(z)e = 0, e = 0\} \tag{23}$$

$$\mathcal{H}_i = \{x \in \mathbb{R}^6 \mid R^\top(z)e = 0, e \neq 0\} \tag{24}$$

respectively. Notice that for planar agents, any 1-D subspace is invariant and the set

$$\mathcal{H}_l = \{x \in \mathbb{R}^6 \mid R^\top(z)e = 0, \text{rank}(Z) = 1\} \tag{25}$$

is one set of undesired equilibria. It can be easily shown that, for a triangle formation, $\mathcal{H}_l = \mathcal{H}_i$. Indeed, if not, for any incorrect formation which is not collinear, the force on some agent will not be balanced. Denote $\eta = \{x \in \mathbb{R}^6 \mid \text{rank}(Z) = 1\}$. In the rest of this section, we shall only refer to $\mathcal{H}_l$ instead of $\mathcal{H}_i$.

The main result is formulated as follows.

*Theorem 8:* Consider the system (8) with initial positions in $\mathbb{R}^2$, then the set $\mathcal{H}_c$ is almost globally stable.

Before we prove Theorem 8, we need the following lemma.

*Lemma 9:* For any equilibria $x^*$ in $\mathcal{H}_l$ with $(1, 3)$ being the longest edge, then we have

$$\|x_1^* - x_2^*\| < d_{12}, \quad \|x_2^* - x_3^*\| < d_{23}, \quad \|x_3^* - x_1^*\| > d_{31}. \tag{26}$$

*Proof:* Note that the dynamic (8) with three agents can be rewritten as

$$\dot{x}_1 = (\rho_1 + \rho_3)(x_2 - x_1) + \rho_3(x_3 - x_2) \tag{27}$$

$$\dot{x}_2 = \rho_1(x_1 - x_2) + \rho_2(x_3 - x_2) \tag{28}$$

$$\dot{x}_3 = \rho_3(x_1 - x_2) + (\rho_2 + \rho_3)(x_2 - x_3). \tag{29}$$

Since $(1, 3)$ is the longest edge, then $x_2^*$ is between $x_1^*$ and $x_3^*$. Equation (28) then implies that at equilibrium, $\rho_1$ and $\rho_2$ have the same sign. Furthermore, (27) and (29) also imply that $\rho_1+\rho_3$ and $\rho_2+\rho_3$ have opposite signs from $\rho_3$. Hence, $\rho_1$ and $\rho_2$ have opposite signs from $\rho_3$. Since $\mathbf{e}_3$ is the longest edge, it can be seen that $\rho_3 < 0$, $\rho_1 > 0$, and $\rho_2 > 0$ cannot hold. Indeed, if that holds, we have $d_{13} > d_{12} + d_{23}$ which violate the triangle inequality. Thus, we conclude that at equilibrium $\rho_1 < 0, \rho_2 < 0$, and $\rho_{31} > 0$ and the conclusion follows. □

*Proof of Theorem 8:* Note that the right-hand side of the system (8) is Lipschitz continuous, together with the fact that the 1-D subspace $\eta$ is invariant, then from any arbitrary initial positions, no trajectories can reach $\eta$ at any finite time. Indeed, if not, then by Picard–Lindelöf theorem [32], the backwards uniqueness of the solution is violated.

Then, if a trajectory, with arbitrary initialization, converges to $\mathcal{H}_l$, it can only converge from $\mathbb{R}^2 \setminus \eta$, i.e., $x(t) \notin \eta, \forall t \geq 0$ and $x(t) \to \mathcal{H}_l$ as $t \to \infty$.

In the following, we prove the trajectories, from any arbitrary initial condition, cannot converge to $\eta$ asymptotically either. We prove this by discussing the possible converging scenarios and contradictions by using perturbation analysis.

It can be seen in the set $\mathcal{H}_l$, that the triangle inequality degenerate to equality. Without loss of generality, we consider the case $\|x_1 - x_2\| + \|x_2 - x_3\| = \|x_3 - x_1\|$ and the function

$$W(t) := \|x_1 - x_2\| + \|x_2 - x_3\| - \|x_3 - x_1\| \tag{30}$$

which is zero when $x_2$ is in the middle of and collinear with $x_1$ and $x_3$ and is positive otherwise.

Here, we shall prove that $W$ does not converge to zero. The dynamic of $W$ is given as

$$\begin{aligned}\frac{dW}{dt} &= \frac{1}{\|x_1 - x_2\|}(x_1 - x_2)^\top(\dot{x}_1 - \dot{x}_2) \\ &\quad + \frac{1}{\|x_2 - x_3\|}(x_2 - x_3)^\top(\dot{x}_2 - \dot{x}_3) \\ &\quad - \frac{1}{\|x_3 - x_1\|}(x_3 - x_1)^\top(\dot{x}_3 - \dot{x}_1) \\ &=: T_1 + T_2 - T_3\end{aligned}$$

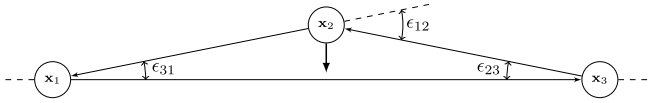


Fig. 16. Illustration of the formation approaching $\mathcal{H}_l$. Arrows on edges describe the defined direction, $\mathbf{x}_1 - \mathbf{x}_2$, ..., and $\epsilon_{ij}$ represent angles between the edges.

where

$$\begin{aligned} T_1 &= -2\rho_1\|x_1 - x_2\| + \rho_2\|x_2 - x_3\|\cos\langle x_1 - x_2, x_2 - x_3\rangle \\ &\quad + \rho_3\|x_1 - x_3\|\cos\langle x_1 - x_2, x_3 - x_1\rangle \\ T_2 &= -2\rho_2\|x_2 - x_3\| + \rho_1\|x_1 - x_2\|\cos\langle x_1 - x_2, x_2 - x_3\rangle \\ &\quad + \rho_3\|x_3 - x_1\|\cos\langle x_3 - x_1, x_2 - x_3\rangle \\ T_3 &= -2\rho_3\|x_3 - x_1\| + \rho_1\|x_1 - x_2\|\cos\langle x_1 - x_2, x_3 - x_1\rangle \\ &\quad + \rho_2\|x_2 - x_3\|\cos\langle x_2 - x_3, x_3 - x_1\rangle. \end{aligned}$$

When $W$ is sufficiently small, we have that the cosines in $T_i, i = 1, 2, 3$ can be approximated by

$$\begin{aligned} \cos\langle x_1 - x_2, x_2 - x_3\rangle &= 1 - \epsilon_{12} \\ \cos\langle x_1 - x_2, x_3 - x_1\rangle &= -1 + \epsilon_{23} \\ \cos\langle x_3 - x_1, x_2 - x_3\rangle &= -1 + \epsilon_{31} \end{aligned}$$

where $\epsilon_{12}, \epsilon_{23}$, and $\epsilon_{31}$ are small positive variables that converge to 0 as $W \to 0$, see Fig. 16 for graphical explanation.

Then, the time derivative of $W$ can be approximated as

$$\begin{aligned} \dot{W} = \|x_1 - x_2\|\rho_1(-\epsilon_{12} - \epsilon_{31}) + \|x_2 - x_3\|\rho_2(-\epsilon_{12} - \epsilon_{31}) \\ + \|x_3 - x_1\|\rho_3(\epsilon_{23} + \epsilon_{31}). \end{aligned}$$

Furthermore, since by Lemma 9, $\rho_1,\ \rho_2 < 0$, and $\rho_3 > 0$, we have $\dot{W} > 0$ whenever $W$ is sufficiently small. We conclude that $W$ does not converge to zero for any arbitrary initialization. Using the same analysis for other equilibria in $\mathcal{H}_l$, we have that for any arbitrary initialization, the trajectory does not converge to $\mathcal{H}_l$. Finally, note that the set $\mathcal{H}_c \cup \mathcal{H}_l$ is the whole equilibria set, then the convergence to $\mathcal{H}_c$ from any arbitrary initial position is proved. □

*Remark 10:* Essentially, the above-mentioned result can be generalized to arbitrary potential functions.

## ACKNOWLEDGMENT

The authors would like to thank Dr. Artur Piotr Zolich, Prof. Jo Arve Alfredsen, and Dr. Ravinder Praveen Kumar Jain for their support during the experiments.

## REFERENCES

[1] A. Zolich *et al.*, "Survey on communication and networks for autonomous marine systems," *J. Intell. Robot. Syst.*, vol. 15, pp. 1–25, May 2017.

[2] A. Zolich, T. A. Johansen, J. A. Alfredsen, J. Kuttenkeuler, and E. Erstorp, "A formation of unmanned vehicles for tracking of an acoustic fish-tag," in *Proc. OCEANS Anchorage*, 2017, pp. 1–6.

[3] M. Breivik, V. E. Hovstein, and T. I. Fossen, "Straight-line target tracking for unmanned surface vehicles," *Model., Identificat. Control, Norwegian Res. Bull.*, vol. 29, no. 4, pp. 131–149, 2008.

[4] P. Tokekar, E. Branson, J. Vander Hook, and V. Isler, "Tracking aquatic invaders: Autonomous robots for monitoring invasive fish," *IEEE Robot. Autom. Mag.*, vol. 20, no. 3, pp. 33–41, Sep. 2013.

[5] Y. Cao, W. Yu, W. Ren, and G. Chen, "An overview of recent progress in the study of distributed multi-agent coordination," *IEEE Trans. Ind. Informat.*, vol. 9, no. 1, pp. 427–438, Feb. 2013.

[6] K.-K. Oh, M.-C. Park, and H.-S. Ahn, "A survey of multi-agent formation control," *Automatica*, vol. 53, pp. 424–440, Mar. 2015.

[7] S. L. Smith, M. E. Broucke, and B. A. Francis, "Stabilizing a multi-agent system to an equilateral polygon formation," in *Proc. 17th Int. Symp. Math. Theory Netw. Syst.*, 2006, pp. 2415–2424.

[8] M. Cao, A. S. Morse, C. Yu, B. D. O. Anderson, and S. Dasguvta, "Controlling a triangular formation of mobile autonomous agents," in *Proc. 46th IEEE Conf. Decision Control*, 2007, pp. 3603–3608.

[9] Z. Sun, U. Helmke, and B. D. O. Anderson, "Rigid formation shape control in general dimensions: An invariance principle and open problems," in *Proc. 54th IEEE Conf. Decision Control (CDC)*, Dec. 2015, pp. 6095–6100.

[10] D. V. Dimarogonas and K. H. Johansson, "On the stability of distance-based formation control," in *Proc. 47th IEEE Conf. Decision Control*, Dec. 2008, pp. 1200–1205.

[11] D. V. Dimarogonas and K. H. Johansson, "Further results on the stability of distance-based multi-robot formations," in *Proc. Amer. Control Conf.*, 2009, pp. 2972–2977.

[12] T. Balch and R. C. Arkin, "Behavior-based formation control for multi-robot teams," *IEEE Trans. Robot. Autom.*, vol. 14, no. 6, pp. 926–939, Dec. 1998.

[13] M. Egerstedt and X. Hu, "Formation constrained multi-agent control," *IEEE Trans. Robot. Autom.*, vol. 17, no. 6, pp. 947–951, Apr. 2001.

[14] Z. Lin, B. Francis, and M. Maggiore, "Necessary and sufficient graphical conditions for formation control of unicycles," *IEEE Trans. Autom. Control*, vol. 50, no. 1, pp. 121–127, Jan. 2005.

[15] M. U. Khan, S. Li, Q. Wang, and Z. Shao, "Formation control and tracking for co-operative robots with non-holonomic constraints," *J. Intell. Robotic Syst.*, vol. 82, no. 1, pp. 163–174, Apr. 2016.

[16] T.-H. Kim and T. Sugie, "Cooperative control for target-capturing task based on a cyclic pursuit strategy," *Automatica*, vol. 43, no. 8, pp. 1426–1431, 2007.

[17] S. H. Dandach, B. Fidan, S. Dasgupta, and B. D. O. Anderson, "A continuous time linear adaptive source localization algorithm, robust to persistent drift," *Syst. Control Lett.*, vol. 58, no. 1, pp. 7–16, Jan. 2009.

[18] M. Deghat, I. Shames, B. D. O. Anderson, and C. Yu, "Target localization and circumnavigation using bearing measurements in 2D," in *Proc. 49th IEEE Conf. Decision Control (CDC)*, Dec. 2010, pp. 334–339.

[19] I. Shames, S. Dasgupta, B. Fidan, and B. D. O. Anderson, "Circumnavigation using distance measurements under slow drift," *IEEE Trans. Autom. Control*, vol. 57, no. 4, pp. 889–903, Apr. 2012.

[20] R. Sharma, S. Quebe, R. W. Beard, and C. N. Taylor, "Bearing-only cooperative localization," *J. Intell. Robot. Syst.*, vol. 72, nos. 3–4, pp. 429–440, Dec. 2013.

[21] M. W. Mehrez, G. K. I. Mann, and R. G. Gosine, "An optimization based approach for relative localization and relative tracking control in multi-robot systems," *J. Intell. Robotic Syst.*, vol. 85, no. 2, pp. 385–408, Feb. 2017.

[22] M.-C. Park, Z. Sun, M. H. Trinh, B. D. O. Anderson, and H.-S. Ahn, "Distance-based control of k4 formation with almost global convergence," in *Proc. IEEE 55th Conf. Decision Control (CDC)*, Dec. 2016, pp. 904–909.

[23] Z. Sun, *Cooperative Coordination and Formation Control for Multiagent Systems*. Cham, Switzerland: Springer, 2018.

[24] B. Bollobás, *Modern Graph Theory*, vol. 184. Cham, Switzerland: Springer, 2013.

[25] P. Monzon, "On necessary conditions for almost global stability," *IEEE Trans. Autom. Control*, vol. 48, no. 4, pp. 631–634, Apr. 2003.

[26] A. Beck, P. Stoica, and J. Li, "Exact and approximate solutions of source localization problems," *IEEE Trans. Signal Process.*, vol. 56, no. 5, pp. 1770–1778, May 2008.

[27] C. K. Batchelor and G. Batchelor, *An Introduction to Fluid Dynamics*. Cambridge, U.K.: Cambridge Univ. Press, 1967.

[28] J. Pinto, P. S. Dias, R. Martins, J. Fortuna, E. Marques, and J. Sousa, "The LSTS toolchain for networked vehicle systems," in *Proc. MTS/IEEE OCEANS*, Jun. 2013, pp. 1–9.

[29] L. Meier. (2013). *Mavlink: Micro Air Vehicle Communication Protocol*. [Online]. Available: https://github.com/mavlink

[30] K. Praveen, H. Praveena, and C. Subhas, "Ecg signal de-noising by using empirical wavelet transform and extended Kalman filter," *Int. J. Pure Appl. Math.*, vol. 120, no. 6, pp. 11983–11996, 2018.

[31] U. Helmke and J. B. Moore, *Optimization and Dynamical Systems*. London, U.K.: Springer-Verlag 1996.

[32] E. A. Coddington and N. Levinson, *Theory of Ordinary Differential Equations*. New York, NY, USA: McGraw-Hill, 1955.

**Rasmus Ringbäck** was born in Stockholm, Sweden, in 1991. He received the B.Sc. degree in electrical engineering and the M.Sc. degree in systems, control and robotics from the KTH Royal Institute of Technology, Stockholm, in 2015 and 2017, respectively.

He worked as a Research Engineer within a project focused on autonomous transport solutions at the Integrated Transport Research Laboratory, KTH Royal Institute of Technology. Since 2018, he has been with the Department Systems Engineering, Saab AB, Järfälla, Sweden, in the field of electronic warfare and airborne surveillance systems.

**Jieqiang Wei** was born in Qufu, China, in 1987. He received the B.Sc. degree in mathematics from Qufu Normal University, Jining, China, the M.Sc. degree in mathematics from Beijing Normal University, Beijing, China, and the Ph.D. degree from the Johann Bernoulli Institute for Mathematics and Computer Science, University of Groningen, Groningen, The Netherlands, in 2016.

From 2016 to 2019, he was a Post-Doctoral Researcher with the Autonomic Complex Communication nEtworks, Signals and Systems Linnaeus Center, School of Electrical Engineering and Computer Science, KTH Royal Institute of Technology, Stockholm, Sweden. He is currently a Data Scientist with Ericsson AB, GAIA, Stockholm. His research interests include networked control systems, reinforcement learning, data science, optimization, nonlinear systems and control, and stochastic systems.

**Elias Strandell Erstorp** (Graduate Student Member, IEEE) received the M.Sc. degree in naval architecture from the KTH Royal Institute of Technology, Stockholm, Sweden, in 2014. He is currently pursuing the Ph.D. degree in acoustic underwater communications with a focus on network protocols. His M.Sc. thesis was on integrating an autonomous surface vehicle (ASV) with the LSTS toolchain for mission handling and vehicle control.

He was a Research Engineer with the KTH Royal Institute of Technology, where he was working with autonomous systems for two years. Most of the work was related to electronics and software in ASVs and an autonomous underwater vehicle. He has been on missions to arctic regions, where he has helped mapping the bathymetry of small lakes using mentioned ASV.

**Jakob Kuttenkeuler** received the Ph.D. degree in aeronautical engineering in 1998.

He is currently a Full Professor in naval architecture with the Centre for Maritime Robotics, KTH Royal Institute of Technology, Stockholm, Sweden. He is also a Senior Member with the Swedish Maritime Research Centre, KTH Royal Institute of Technology, where his research focuses on the fields of autonomous underwater vehicles. He has dedicated his research efforts into various fields ranging from lightweight design, aircraft composites, aeroelastics, robotic sailing, ocean monitoring, and maritime robotics.

**Tor Arne Johansen** (Senior Member, IEEE) received the M.Sc. and Ph.D. degrees in electrical and computer engineering from the Norwegian University of Science and Technology, Trondheim, Norway, in 1989 and 1994, respectively.

From 1995 to 1997, he was a Researcher SINTEF, Trondheim, Norway. He was appointed as an Associate Professor with the Norwegian University of Science and Technology (NTNU), Trondheim, in 1997, where he was appointed as a Professor in 2001. In 2002, he co-founded the company Marine Cybernetics AS, Trondheim, where he was the Vice President until 2008. He is currently a Principal Researcher within the Center of Excellence on Autonomous Marine Operations and Systems (NTNU-AMOS) and the Director of the Unmanned Aerial Vehicle Laboratory, NTNU, and the SmallSat Laboratory. He recently co-founded the spin-off companies Scout Drone Inspection, Trondheim, UBIQ Aerospace, Trondheim, and Zeabuz, Trondheim. He has authored and coauthored several hundred articles in the areas of control, estimation, and optimization with applications in the marine, aerospace, automotive, biomedical, and process industries.

Prof. Johansen received the 2006 Arch T. Colwell Merit Award of the SAE.

**Karl Henrik Johansson** (Fellow, IEEE) received the M.Sc. and Ph.D. degrees from Lund University, Lund, Sweden.

He has held visiting positions with the University of California of Berkeley, Berkeley, CA, USA, California Institute of Technology, Pasadena, CA, Nanyang Technological University, Singapore, Institute of Advanced Studies, Hong Kong University of Science and Technology, Hong Kong, and Norwegian University of Science and Technology, Trondheim, Sweden. He is currently the Director of the Stockholm Strategic Research Area ICT The Next Generation and a Professor of the School of Electrical Engineering and Computer Science, KTH Royal Institute of Technology, Stockholm, Sweden. His research interests are in networked control systems, cyber-physical systems, and applications in transportation, energy, and automation.

He is a fellow of the Royal Swedish Academy of Engineering Sciences. He is an IEEE Distinguished Lecturer. He is a member of the IEEE Control Systems Society Board of Governors, the IFAC Executive Board, and the European Control Association Council. He has received several best paper awards and other distinctions. He is a Distinguished Professor with the Swedish Research Council and a Wallenberg Scholar. He has received the Future Research Leader Award from the Swedish Foundation for Strategic Research and the triennial Young Author Prize from IFAC.